The Principle of the Micro-Electronic Neural Bridge and a Prototype System Design

Zong-Hao Huang, Zhi-Gong Wang, *Senior Member, IEEE*, Xiao-Ying Lü, Wen-Yuan Li, Yu-Xuan Zhou, Xiao-Yan Shen, and Xin-Tai Zhao

***Abstract*—The micro-electronic neural bridge (MENB) aims to rebuild lost motor function of paralyzed humans by routing movement-related signals from the brain, around the damage part in the spinal cord, to the external effectors. This study focused on the prototype system design of the MENB, including the principle of the MENB, the neural signal detecting circuit and the functional electrical stimulation (FES) circuit design, and the spike detecting and sorting algorithm. In this study, we developed a novel improved amplitude threshold spike detecting method based on variable forward difference threshold for both training and bridging phase. The discrete wavelet transform (DWT), a new level feature coefficient selection method based on Lilliefors test, and the k-means clustering method based on Mahalanobis distance were used for spike sorting. A real-time online spike detecting and sorting algorithm based on DWT and Euclidean distance was also implemented for the bridging phase. Tested by the data sets available at Caltech, in the training phase, the average sensitivity, specificity, and clustering accuracies are 99.43%, 97.83%, and 95.45%, respectively. Validated by the three-fold cross-validation method, the average sensitivity, specificity, and classification accuracy are 99.43%, 97.70%, and 96.46%, respectively.**

***Index Terms*—Functional electrical stimulation, k-means clustering, Lilliefors test, Mahalanobis distance, micro-electronic neural bridge, motor function rebuilding, spike detecting, spike sorting, spinal cord injury.**

I. Introduction

THE second leading cause of paralysis is spinal cord injury (SCI). According to the survey conducted by the Reeve Foundation in 2009, approximately 0.4% of the U.S. population or about 1 275 000 people was reported to be paralyzed due to SCI [1]. Accordingly, the total number of paralyzed people in the world would be more than 20 million.

Substantial neural function rebuilding of injured spinal cord should rely on biomedical methods. In general, they can be mainly categorized into three different techniques.

The first one focused on enhancing the neural regeneration in central nervous system including the neutralization of potential growth inhibitory molecules [2], [3], the transplantation of cells or tissue that support axonal elongation, such as peripheral nerve [4], [5], fetal central nervous system cells [6], Schwann cell [7], [8], olfactory ensheathing cell [9], [10], embryonic stem/progenitor cells [11], and adult stem/progenitor cells [12], the delivery of diffusible factors that are known to promote axonal growth, such as neurotrophic factors [13], [14], gene therapy [15], [16], and combination strategies of the above methods [17], [18]. However, there are many difficulties with the technique of category one, such as the optimal source of cells, age of cells, graft strategy, and timing of intervention [10], [11], [19], [20]. Additionally, the efficacy is still controversial [21]–[23]. In this sense, there is quite a lot further work to be done to ascertain the safety and efficacy of this type of method [24].

The second category is based on physical therapy or rehabilitative training, including upper-extremity exercise, body-weight-supported treadmill training [25], [26], and robotic or manually assisted training [27]–[29]. Techniques of this category can improve the inherent physical capability of the patients based on the fact that after SCI, the spinal circuitry below the lesion site maintains active and functional neuronal properties and can respond to extrinsic input from below the level of the injury. It can generate oscillating coordinated motor patterns and is capable of considerable plasticity [30], [31]. However, the mechanisms for physical therapy or rehabilitative training need to be better understood for rational improvement in therapy [24]. Inappropriate therapy may result in special risk to people with SCI, including autonomic dysreflexia, fracture or muscular injury, and hyperthermia [32].

The third category method aims to replace or rebuild the lost functions by using electronic or mechanical devices such as exoskeleton [33], functional electrical stimulation (FES) [34], and brain-computer interface (BCI) [35], [36]. However, for this category, there are still many challenges from the engineering standpoint, such as design of implantable device, signal processing algorithm, weak signal detection, and power reduction.

In this study, we developed a novel method aiming to restore the motor function of the paralyzed limbs from the perspective of communication. This study focused on the proto-

Manuscript received November 16, 2014; revised June 10, 2015; accepted July 28, 2015. Date of publication August 12, 2015; date of current version January 06, 2016. This work was supported by the National Natural Science Foundation of China under Grant 90307013 and Grant 90707005 and by the Science and Technology Pillar Program of Jiangsu Province under Grant BE2013706. *Corresponding author: Z.-G. Wang* (e-mail: zgwang@seu.edu.cn).

Z.-H. Huang and X.-T. Zhao are with the Institute of RF & OE-ICs, Southeast University, Nanjing, China (e-mail: hzh_seu@aliyun.com).

Z.-G. Wang and W.-Y. Li are with the Institute of RF & OE-ICs, Southeast University, Nanjing, China, and also with the Co-Innovation Center of Neuroregeneration, Nantong University, Nantong JS 226001, China.

X.-Y. Lü is with the State Key Lab of Bioelectronics, Southeast University, Nanjing, China, and also with the Co-Innovation Center of Neuroregeneration, Nantong University, Nantong JS 226001, China.

Y.-X. Zhou is with the State Key Lab of Bioelectronics, Southeast University, Nanjing, China.

X.-Y. Shen was with the Institute of RF & OE-ICs, Southeast University, Nanjing, China. She is now with the School of Electronic Information, Nantong University, Nantong, China, and also with the Co-Innovation Center of Neuroregeneration, Nantong University, Nantong JS 226001, China.

Color versions of one or more of the figures in this paper are available online at http://ieeexplore.ieee.org.

Digital Object Identifier 10.1109/TNSRE.2015.2466659

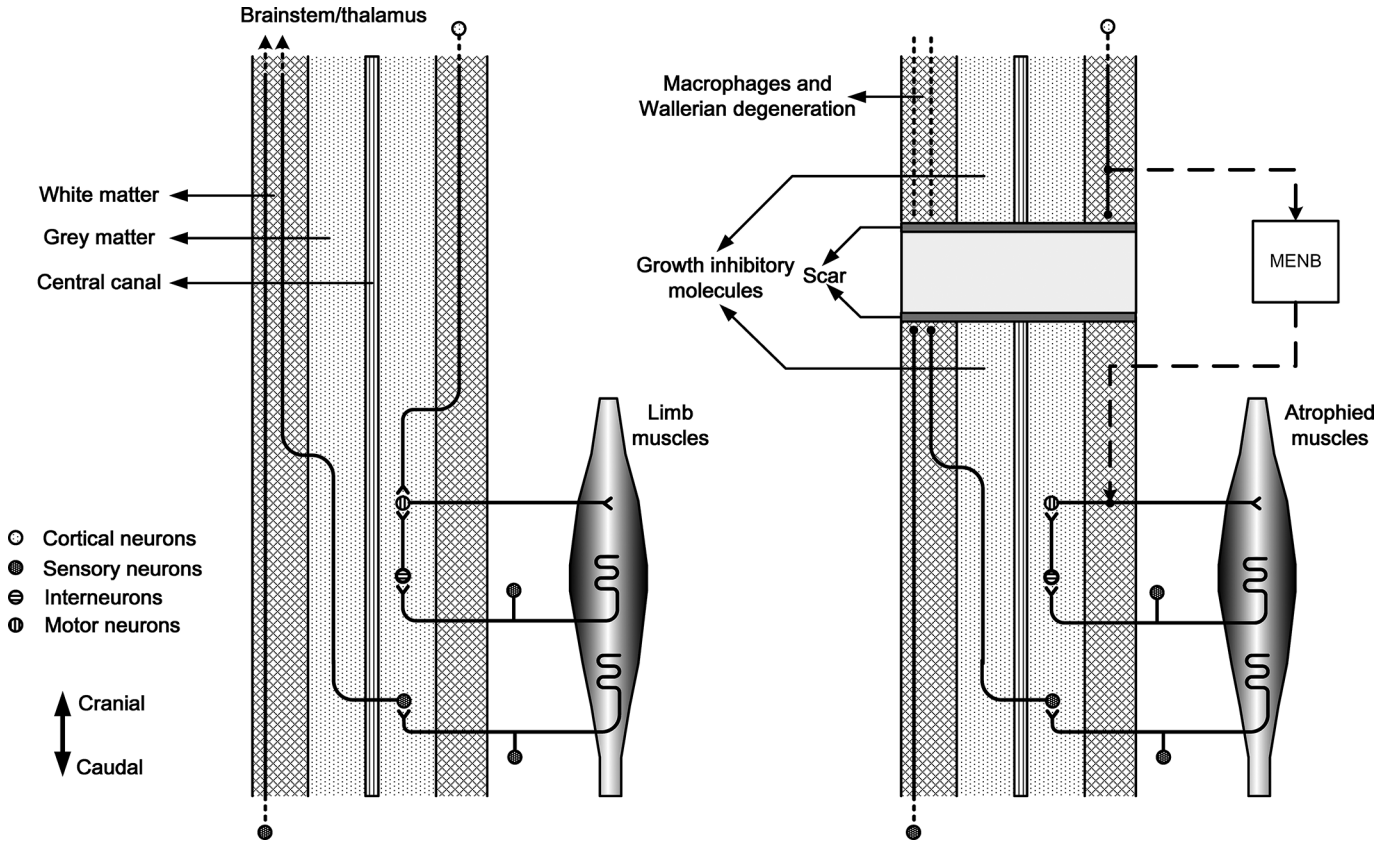

Fig. 1. Illustration of the MENB. (a) Simplified sagittal view of the intact spinal cord. (b) Simplified sagittal view of the complete spinal cord transection and the concept of MENB.

type system design of this method, including the key algorithms: spike detecting and sorting. This paper is organized as follows: Section II describes the methodology and system architecture (the principle of our method, system overview, hardware description, spike detection/sorting, stimulating electrode configuration). Section III validates the proposed signal processing algorithm. Section IV summarizes and concludes the paper.

II. Methods and System

A. Method Based on Communication

The information interaction process between the brain and other parts of the body can be analogy to a communication process. In this process, the brain can be analogy to a central computer along with a series of transceivers which transmit the instructions to the effectors and receive information from the receptors. The effector can be analogy to a receiver, which receives the instructions from the brain. The receptor can be analogy to a transmitter, which transmits the acquired information to the brain. Part of the neural system such as the white matter in spinal cord and peripheral nervous, plays a role of the communication channels for neural signal transmission. Therefore, we can simply describe the mechanism of limb paralysis caused by SCI as the signals cannot be communicated between the brain and the effectors (the muscles), due to the neural channel interruption. By techniques of the brain-computer interface (BCI), electroencephalography (EEG) or electrocorticogram (ECoG) signals are used to decode the intention of the patients and further to control the prosthetic devices [36]. In this technique, the challenge lies in decoding the intention of the patients.

In order to reduce the difficulty of intention decoding, we have developed a novel concept named micro-electronic neural bridge (MENB) based on the principles of communication and functional electrical stimulation (FES) technique for neural signal regeneration and motor function rebuilding of paralyzed limbs [37]. The main idea of the MENB can be briefly described as follows.

In Fig. 1(a), it is a sagittal view of the intact spinal cord [24]. Cortical, brainstem, and spinal axons project to motor neurons in spinal cord gray matter, which in turn send axons through peripheral nervous system (PNS) to the target effectors, i.e., the muscles. At the same time, primary sensory axons send axons through PNS to second order sensory neurons in the spinal cord gray matter, which in turn send axons through white matter to the brainstem and thalamus. Neural circuitry formed by the sensory neuron, the interneuron, and motor neuron has been presented in Fig. 1 as well.

Take the complete spinal cord transection for example. The concept of the MENB can be illustrated in Fig. 1(b). After the complete spinal cord injury, many cells die immediately, as well as progressively. Some cells from PNS often invade the injury site to form a connective tissue scar incorporating astrocytes, progenitor cells, and microglia, which secrete many neuro-developmental inhibitor molecules and prevent complete recovery of the injured central nervous system (CNS). Many

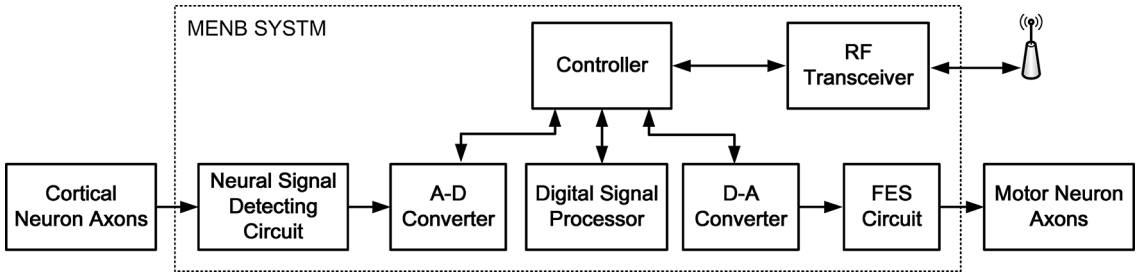

Fig. 2. Block diagram of the MENB prototype system for motor function rebuilding.

ascending and descending axons are interrupted and fail to regenerate over long distance. However, the motor neurons sending axons through PNS to muscles are still alive, as well as the cortical neurons. The MENB is a microelectronic system which bypasses the interrupted axons and forms new signal channels between the cortical neurons and the motor neurons. In this way, muscle contraction of paralyzed limbs can be produced by the neural impulses generated by cortical neurons, and the motor function of paralyzed limb can be rebuilt.

The concept of the MENB is based upon two facts: 1) the mammalian axons can be approximately considered to act as digital signaling devices, conveying information only by the timing and rate of all-or-none action potentials [38]; 2) the action potentials can be generated by electrical stimulation [39]. Therefore, based on communication principle, an MENB acts as multiple point-to-point relays in the neuron communication system which detects action potentials from the axons of cortical neurons in the white matter, generates electrical stimulating signals based on the spike detecting and sorting algorithm, and applies the stimuli on the axons of motor neurons to initiate new action potentials for producing muscle contraction. In this way, the motor function of the paralyzed limb can be rebuilt.

In the following section of this study, the MENB prototype system design will be discussed in detail.

B. MENB Prototype System Overview

The block diagram of the MENB prototype system is shown in Fig. 2. The system includes a neural signal detecting circuit, an analog to digital (A-D) converter, a digital signal processor, a digital to analog (D-A) converter, an FES circuit, an RF transceiver, and a controller. The neural signal is recorded from the cortical neural axons by means of extracellular recording. The great advantage of the extracellular recording is that the activity of neurons can be recorded without having to impale and consequently damage them. The recorded neural signal is amplified and filtered by the neural signal detecting circuit. Then, the signal is converted to a digital one and transferred to a digital signal processor under the control of the controller. The spike detecting and sorting algorithms are performed in the digital signal processor and the results are returned back to the controller. According to the results, a D-A converter outputs stimuli to the FES circuit for stimulation. At the same time, the digital signal can be transmitted wirelessly to a PC for further off-line analysis.

The data flowchart and the waveforms of each step are shown in Fig. 3. At first, the neural signal from the cortical neural

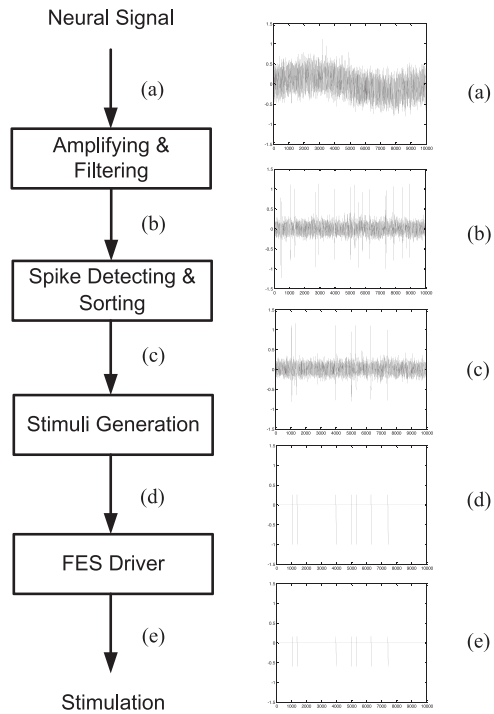

Fig. 3. MENB data flowchart and waveforms of each step.

axons [indicated as Fig. 3(a)] is amplified and filtered by the neural signal detecting circuit. After amplifying and filtering, the signal-to-noise ratio (SNR) is improved and the low frequency drift is eliminated as Fig. 3(b). Because the spikes from different neurons are recorded by the same electrode, the spike detecting and sorting algorithms are performed, and spikes from one neuron, which is to be bridged, are selected [indicated as Fig. 3(c)]. A stimulating pulse train is generated according to the selected spike train [indicated as Fig. 3(d)]. Considering the effective action potential initiation and tissue damage, a charge balanced biphasic slow reversal waveform is used for the stimulation. Finally, the pulse train is converted to a current signal for FES [indicated as Fig. 3(e)], which will be applied on the motor neuron axons.

C. Hardware Description

The neural signal detecting circuit and FES circuit design based on discrete components has been discussed in literature

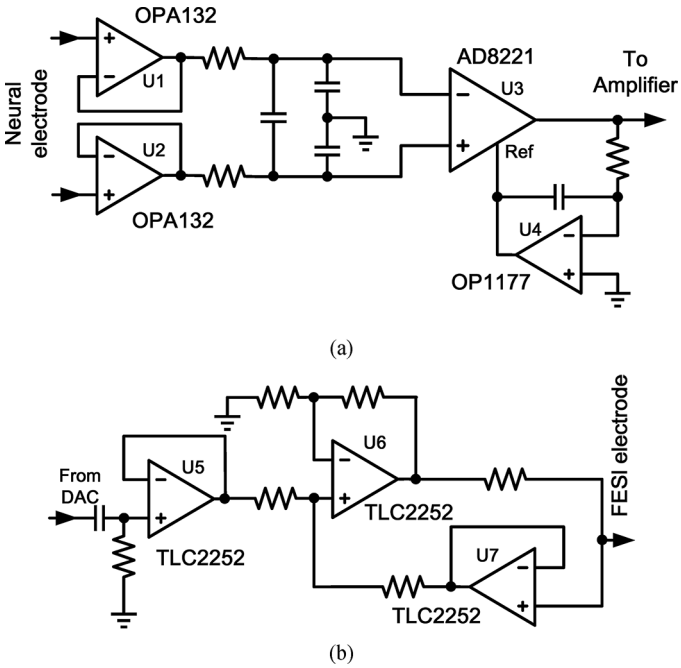

Fig. 4. (a) Neural signal detecting circuit schematic diagram. (b) FES circuit schematic diagram.

TABLE I
NEURAL SIGNAL DETECTING CIRCUIT PARAMETERS

Parameter	Value	Units
Supply voltage	±3	V
Quiescent current	9.38	mA
Quiescent dissipation	56.28	mW
Gain(adjustable)	40 to 80	dB
Input impedance(differential)	$10^{13}\|\|2$	Ω||pF
Input noise voltage @1kHz	24	nV/$\sqrt{\text{Hz}}$
CMRR with 1kΩ source imbalance @1kHz	138	dB
PSRR@100Hz	80	dB
Band width	0.3 to 3	kHz

[40] and the schematic representations of the circuits are shown in Fig. 4.

In Fig. 4(a), the FET-input operational amplifier OPA132 with high input impedance is used as the buffer stage, based on the fact that high input impedance benefits the interference reduction [41]. Because much interference can be viewed as common-mode voltage inputs, an instrumental amplifier with a high common mode reject ration (CMRR) has been used. In the front of the instrumental amplifier, there is an RF filtering network for the radio frequency interference (RFI) rectification errors reduction, considering the fact that many instrumental amplifiers have virtually no CMRR above 20 kHz [42]. The RF filtering network is especially important for a weak signal detecting circuit with RF transceiver. The parameter design of the network depends on the CMRR characteristic of the instrumental amplifier. Based on the datasheets of the used chips and the SPICE model simulation, the parameters of the neural signal detecting circuit is presented in Table I.

The schematic diagram of the FES circuit is presented in Fig. 4(b). The D-A converter generates charge balanced biphasic slow reversal waveform for stimulation. There are

TABLE II
FUNCTIONAL ELECTRICAL STIMULATION CIRCUIT PARAMETERS

Parameter	Value	Units
Supply voltage	±3	V
Quiescent current	0.48	mA
Quiescent dissipation	2.88	mW
Transconductance	2	mS
Max output current	±3	mA
Minimal current step	0.023	mA
Compliance voltage	-3 to 2	V
Output impedance	2×10^{6}	Ω
PSRR@100Hz	80	dB
High pass cutoff frequency	7.23	Hz

two phases for the stimulating waveform: the stimulating (first) phase and the reversal (second) phase. The stimulating phase initiates the desired action potential, and the reversal phase is used to reverse the direction of electrochemical processes occurring during the stimulating phase. We use a negative pulse with a width of 500 μs as the stimulating phase, and a positive pulse with four times the negative pulse's width but one fourth the negative pulse's amplitude as the reversal phase. In Fig. 4(b), two low-power, rail-to-rail and low-input offset/bias current amplifiers TLC2252 (U6 and U7) comprise the voltage-current converters for stimulation, considering the advantage of a current-source-based stimulator [43]. Based on the datasheets and the SPICE model simulation, the parameters of the FES circuit is presented in Table II.

The mixed signal micro-controller MSP430F169 is used as the controller in Fig. 2. In this micro-controller, 8-channel 12-bit analog-to-digital converters (ADCs) and 2-channel 12-bit digital-to-analog converters (DACs) are integrated. A digital media processor DM3730 (1 GHz ARM Cortex™-A8 core and 800 MHz TMS320C64x+™ DSP Core) with Ubuntu 11.04 operational system is used as the digital signal processor for spike detecting and sorting algorithm. A 2.4-GHz low cost transceiver CC2500 programmed at the data rate 500 kb/s is used as the RF transceiver for off-line data recording and analysis. The controller, the digital signal processor, and the RF transceiver exchange their data through a serial peripheral interface (SPI).

D. Spike Detection

Several methods for spike detection have been reported in literature including amplitude threshold [44], window detection [45], teager energy operator (TEO) [46] and multiresolution TEO (MTEO) [47]. In this study, we proposed an improved amplitude threshold method for the spike detection. $x(n)$ is the A-D converter output signal with a sample rate at 24 kHz. Take the positive threshold for example, if $x(n)$ satisfy

$$\begin{cases} x(i) \geq \text{thr}, x(i-1) < \text{thr} \\ x(i) - x(i-1) > \frac{\alpha}{\sigma_{\text{n}}} \end{cases} \tag{1}$$

a spike time will be marked, and a frame of 64 samples (approximately 2.7 ms) around the spike time will be fetched from $x(n)$ with the maximal value at data point 20. Here we chose a frame of 64 (2^6) samples, because it is convenient for the further discrete wavelet transform (DWT), and the frame duration is similar to the action potential duration.

In (1), thr is the amplitude threshold which can be calculated by

$$\text{thr} = \begin{cases} 3\sigma_{\text{n}} & \text{in bridging phase} \\ 4\sigma_{\text{n}} & \text{in training phase} \end{cases}. \tag{2}$$

Note that thr is different depending on the system phase. The reason for different thr will be explained in Section III.

In (1), parameter a is a constant and needs to be chosen depending on the recorded data. Define set $\boldsymbol{I}$:

$$\boldsymbol{I} = \{i | x(i) \geq \text{thr}, x(i-1) < \text{thr}\}. \tag{3}$$

The variable

$$A = \{x(i) - x(i-1)\} \times \sigma_{\text{n}}|_{i \in \boldsymbol{I}}. \tag{4}$$

The parameter a is chosen according to the distribution of A which will be presented in Section III.

As in (1), (2) and (4), σ_{n} is the background noise standard deviation, which can be estimated by (5) as in [48]

$$\sigma_{\text{n}} = \text{median}\left\{\frac{|x|}{0.6745}\right\}. \tag{5}$$

The first inequality constraint in (1) is the amplitude constraint according to the amplitude threshold method. $x(i)$ is the first data point that exceeds the amplitude threshold. The forward difference of $x(i)$ indicates the tendency that the spike exceeds the amplitude threshold. Note that the true spike exceeds the amplitude threshold with a strong tendency when the background noise is low. When the background noise increases, true spike exceeds the amplitude threshold with a less strong tendency than in the low background noise situation. Therefore, a variable forward difference threshold which is inversely proportional to the background noise standard deviation has been chosen as the second inequality constraint in (1). Results of the improved method compared with the traditional amplitude threshold method will be presented in Section III.

E. Spike Sorting

The system has two phases of operation for spike detecting and sorting: the training phase and the bridging phase. In the training phase, recorded data was transmitted by the RF transceiver and analyzed off-line. In this phase, spike frames were firstly obtained based on the method mentioned in spike detection section. Then, a four-level decomposition DWT with Haar wavelets was implemented for each frame. We chose the Haar wavelets due to their compact support, orthogonality, which allows the discriminative features of the spikes to be expressed with few wavelet coefficients [44], and the low computational complexity for real-time processing. We selected the feature coefficients from the 64 wavelet coefficients acquired by the DWT, according to the probability distribution of the coefficients. A good coefficient for distinguishing different spike shapes should have a multimodal distribution and the least Gaussian distribution [49]. Therefore, Lilliefors test (L-test) [50] for normality was used for the coefficient selection. The selected coefficients formed a new feature vector for each frame. Then, K-means clustering method was used based on the new feature vector, and the cluster number was determined by the elbow method [51]. We chose the K-means method because of its simplicity and speed which is very appealing in practice. After the clustering operation, the average feature vector for each class was calculated as the class feature vector which will be used in the bridging phase.

In the bridging phase, spike detecting and sorting algorithms were performed on-line in real time by the digital signal processor DM3730. Parameters for the bridging phase, such as background noise standard deviation, class feature vectors, and selected wavelet coefficients, were obtained in the training phase. DWT was performed on the spike frames using a real time DWT algorithm—pyramidal filter bank algorithm [52]. Then, the feature vector for each frame was generated according to the selected wavelet coefficients. The Euclidean distances or the Mahalanobis distance between the frame feature vector and each class feature vector were calculated. The detected spike was classified to the nearest class measured by the Euclidean distance or the Mahalanobis distance. If the minimal distance exceeds a threshold, the spike will be marked as false detection, and belong to no class. Only the spikes belonging to the neuron to be bridged will generate stimulating waveforms for further stimulation.

The data flow in both the training phase and the bridging phase is shown in Fig. 5. Note that in the training phase, it is an unsupervised clustering problem, whereas it is a classification problem in the bridging phase. The results of the spike sorting algorithm will be presented in Section III. In this study, we did not consider the spike overlap situation for spike detecting and sorting due to the difficulty of this problem [53].

F. Stimulating Electrode Configuration

The stimulating electrode configuration for the MENB has also been studied in literature [54]. According to the simulation results based on a transient finite-element model, a penta-polar electrode configuration with one stimulating electrode in the center and four ground electrodes around the stimulating electrode was proved to be more efficient than mono-polar, bi-polar and tri-polar configurations. This means that the FES circuit needs the smallest current to initiate the action potential with this configuration, which is important for avoiding electrode and tissue damage.

III. Results and Discussion

In order to evaluate the performance of the spike detecting algorithm, two statistical measures—sensitivity (S_{n}) and specificity (S_{p})—were calculated. S_{n} measures the proportion of the correctly identified spikes in all actual spikes, and S_{p} measures the proportion of the actual spikes in all identified spikes. The definitions are as follows:

$$S_{\text{n}} = 1 - \frac{N_{\text{n}}}{N_{\text{t}}} \tag{6}$$

$$S_{\text{p}} = 1 - \frac{N_{\text{p}}}{N_{\text{d}}}. \tag{7}$$

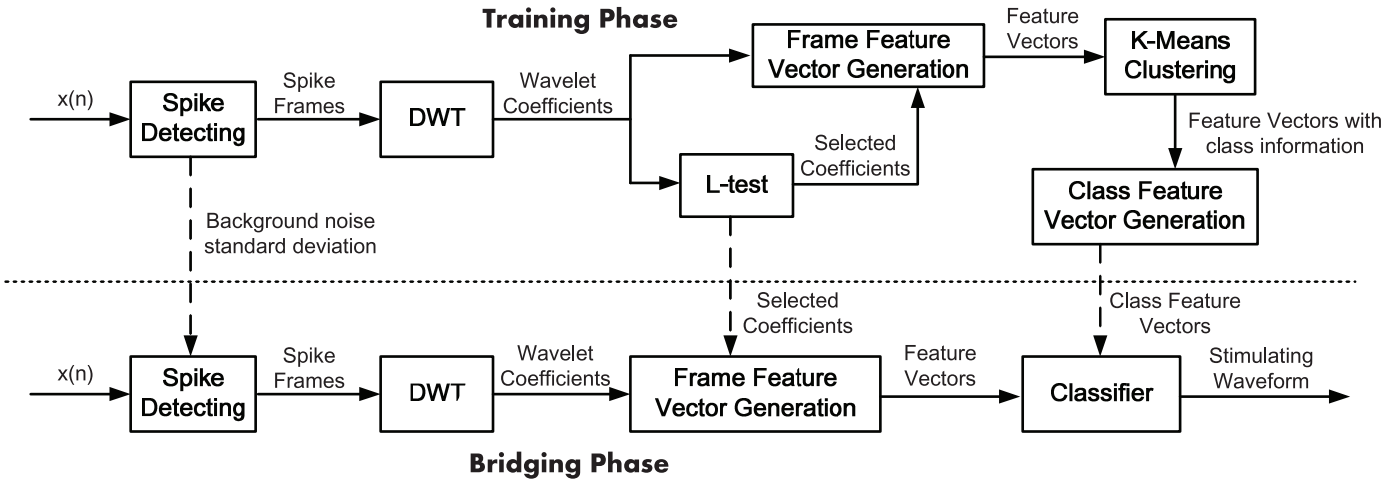

Fig. 5. Data flowchart of the training and bridging phase. In the training phase, parameters for the acquisition phase, such as background noise standard deviation, selected coefficients, and class feature vectors, are obtained (as the dotted line arrow indicates). In the bridging phase, only the spikes belonging to the neuron to be bridged will generate stimulating waveforms for further stimulation.

In (6) and (7), N_{n} is the missing detected spike number, N_{t} is the actual spike number, N_{p} is the false detected spike number, and N_{d} is the detected spike number.

Quiroga posted a database of simulated signals with various background noise standard deviation (0.05, 0.10, 0.15, and 0.20) as well as different wave shapes (three waveforms in each data set), when he was at Caltech. There are a total of four data sets: two easy and two hard. The database was referenced in his study [44] and available at [55]. In this study, Quiroga's database has been used for evaluating the performance of spike detecting and sorting algorithm. The results of three amplitude threshold methods have been presented in Table III. The selection of the amplitude threshold is a tradeoff between S_{n} and S_{p}. The comparison between $thr = 3\ \sigma_{\mathrm{n}}$ and $thr = 4\ \sigma_{\mathrm{n}}$ (Amplitude threshold method) in Table III indicates that lower threshold leads to a higher S_{n} but a lower S_{p}. However, with the improved amplitude threshold method proposed in this paper, the S_{p} is also improved compared to the traditional amplitude threshold method at the same threshold, especially in low background noise situations. Take Easy 1 (noise level 0.05) and Hard 1 (noise level 0.05) for example. In order to determine the parameter a in (1), the value distribution of A (defined by (4)) has been calculated and presented in Fig. 6. Here, we assumed that values near zero are caused by false positives, since these values indicate weak tendency when the spike amplitude equals the amplitude threshold considering the influence of background noise standard deviation. We chose a 0.005 for all the data sets for simplicity.

In the spike detection section, we have mentioned that different amplitude thresholds were used in different phases. This is because the class feature vectors were obtained in the training phase. However, the false positives acted as noise for the class feature vectors generation. Therefore, in the training phase, $4\sigma_{\mathrm{n}}$ was used as the amplitude threshold, based on the fact that S_{p} is more important than S_{n} in this phase. As in the bridging phase, in order to keep a high S_{n}, $3\sigma_{\mathrm{n}}$ was used. In this phase, the distance between the spike frame vector and the class feature vectors can also be used to distinguish the false positives, as the minimal distance between the false positive feature vector and class feature vector often exceeds the distance threshold.

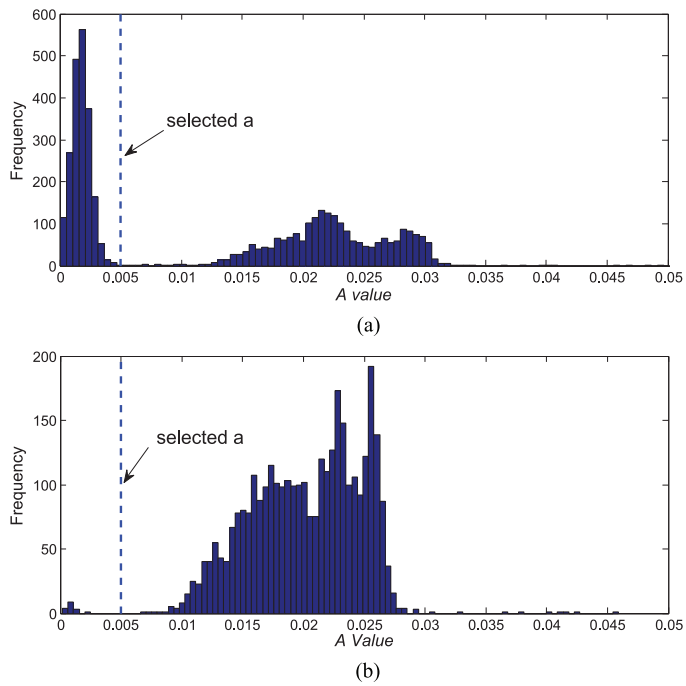

Fig. 6. Value distribution of A and selected parameter a (a) Easy 1 noise level 0.05. (b) Hard 1 noise level 0.05.

Take the Easy 1 (noise level 0.05) data set for example. The spike frames were obtained based on the improved amplitude threshold method, as shown in Fig. 7(a). Fig. 7(b) shows the wavelet coefficients after DWT. The coefficients are organized in a last approximation A4 (Coefficients 1 to 4) and detail levels D1-D4 (D4: Coefficients 5 to 8; D3: Coefficients 9 to 16; D2: Coefficients 17 to 32; D1: Coefficients 33 to 64). For clarity, wavelet coefficients of different classes have been presented in different colors. Feature coefficients selection was

TABLE III
SPIKE DETECTING RESULTS

Data Set	Noise Level	Number of Spikes	Amplitude Threshold (thr=4σ_n)[a]				Amplitude Threshold (thr=3σ_n)				Improved Amplitude Threshold (thr=3σ_n)			
			Misses	FPs[b]	S_n(%)	S_p(%)	Misses	FPs	S_n(%)	S_p(%)	Misses	FPs	S_n(%)	S_p(%)
Easy 1	0.05	3514(785)	17(193)	711	99.38	79.23	0(90)	1113	100	74.77	0(217)	27	100	99.18
Easy 1	0.10	3522(769)	2(177)	57	99.93	97.97	0(138)	337	100	90.77	0(199)	40	100	98.80
Easy 1	0.15	3477(784)	145(215)	14	94.62	99.45	0(202)	176	100	94.83	0(218)	151	100	95.52
Easy 1	0.20	3474(796)	714(275)	10	73.34	99.49	11(213)	198	99.59	94.06	11(219)	197	99.59	94.08
Easy 2	0.05	3410(791)	0(174)	0	100	100	0(79)	393	100	89.25	0(230)	0	100	100
Easy 2	0.10	3520(826)	0(191)	2	100	99.93	0(195)	134	100	96.09	0(234)	17	100	99.48
Easy 2	0.15	3411(763)	10(173)	1	99.62	99.96	1(198)	108	99.96	96.73	1(212)	99	99.96	96.99
Easy 2	0.20	3526(811)	376(256)	5	86.15	99.79	104(256)	95	96.17	97.07	104(265)	86	96.17	97.34
Hard 1	0.05	3383(767)	1(210)	63	99.96	97.65	0(151)	277	100	91.88	0(237)	20	100	99.36
Hard 1	0.10	3448(810)	0(191)	10	100	99.62	0(206)	98	100	97.04	0(230)	21	100	99.35
Hard 1	0.15	3472(812)	8(203)	6	99.70	99.77	0(230)	85	100	97.43	0(239)	76	100	97.70
Hard 1	0.20	3414(790)	184(219)	2	92.99	99.92	21(241)	152	99.20	95.30	21(246)	156	99.20	95.17
Hard 2	0.05	3364(829)	0(182)	1	100	99.96	0(129)	150	100	95.46	0(233)	15	100	99.52
Hard 2	0.10	3462(720)	0(152)	5	100	99.82	0(170)	73	100	97.81	0(200)	15	100	98.54
Hard 2	0.15	3440(809)	3(186)	4	99.89	99.85	0(234)	98	100	97.02	0(244)	92	100	97.19
Hard 2	0.20	3493(777)	262(228)	2	90.35	99.92	109(248)	102	95.99	96.83	109(261)	93	95.99	97.10
Average					96.00	98.27			99.43	93.90			99.43	97.83

Notes: Values in brackets are for overlapping spikes. Overlapping spikes are not considered for the S_n and S_p calculation
[a]Quiroga used this method in his study, results are obtained from his study [44]
[b]FPs is the abbreviation for False Positives

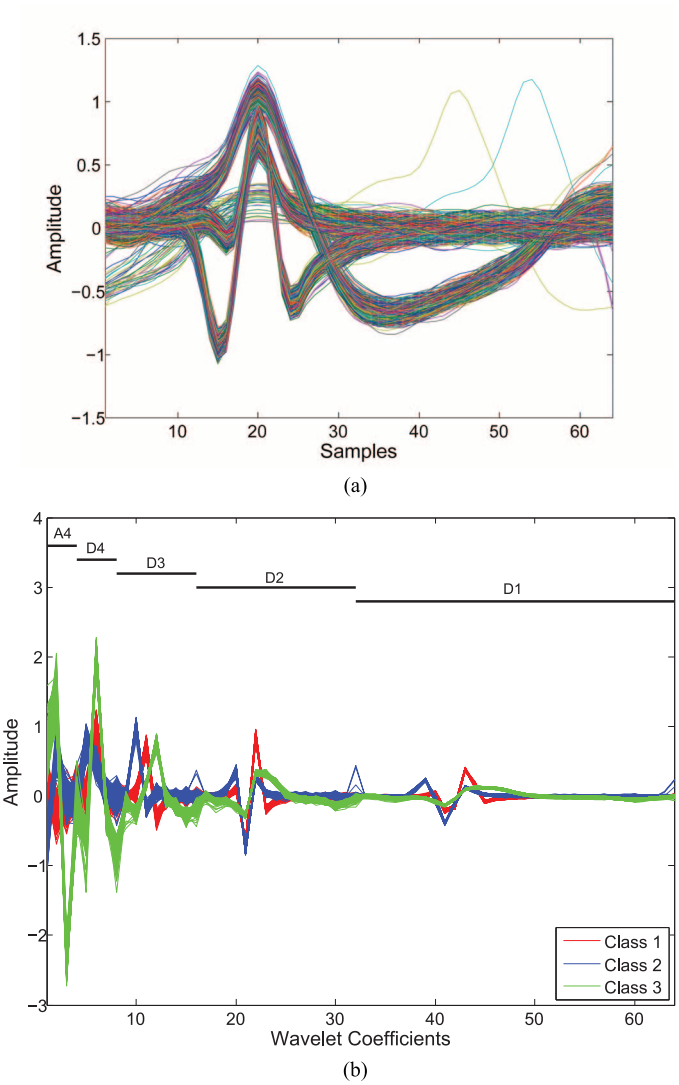

Fig. 7. (a) Obtained spike frames (overlapping spikes are not included). (b) Wavelet coefficients of the spike frames (overlapping spikes and false positives are not included).

TABLE IV
FEATURE COEFFICIENT CANDIDATES FOR EACH DATA SET

Data Set (Noise)	Wavelet Coefficient Number				
	A4	D4	D3	D2	D1
Easy 1(0.05)	**3**	**8**	**10,12**	**22,21,30,23**	**43,39,38,60,41,47,46,40**
Easy 1(0.10)	**3**	**8**	**10,12**	**22,21,23,20**	**43,39,38,41,42,46,40,45**
Easy 1(0.15)	**3**	**6**	**10,11**	**22,21,23,20**	**43,39,41,38,42,45,46,40**
Easy 1(0.20)	**3**	**6**	**10,11**	**22,21,23,20**	**43,39,41,42,38,46,45,47**
Easy 2(0.05)	**3**	7	**10**,14	**19,21,22,20**	**41,38,39,43,40,48,37,36**
Easy 2(0.10)	**3**	7	**10,11**	**21,19,20,22**	**41,38,39,40,43,42,37,48**
Easy 2(0.15)	2	6	**10,11**	**21,20,19,22**	**41,38,39,40,43,42,37,55**
Easy 2(0.20)	1	**7**	**11,10**	**21,20,19,22**	**41,39,40,38,43,42,37,54**
Hard 1(0.05)	**3**	**6**	**11,10**	**22,21,23,20**	**39,45,43,41,40,46,44,58**
Hard 1(0.10)	2	**6**	**11,10**	**22,21,20,23**	**39,43,45,40,41,33,35,62**
Hard 1(0.15)	2	**6**	**11,13**	**21,22,17,23**	**43,39,45,40,42,33,34,41**
Hard 1(0.20)	2	**6**	**11,9**	**21,22,18,23**	**43,42,41,44,45,39,34,35**
Hard 2(0.05)	**2**	**6**	**11,10**	**20,22,21,25**	**41,37,44,40,49,39,50,45**
Hard 2(0.10)	**2**	**6**	**11,10**	**20,22,21,19**	**41,40,44,39,37,43,42,38**
Hard 2(0.15)	2	**6**	**11,10**	**20,21,22,19**	**41,44,40,39,43,37,42,64**
Hard 2(0.20)	**2**	**6**	**11,10**	**21,22,20,17**	**41,44,40,43,37,39,42,62**

Notes: Numbers in bold are the selected feature coefficients

based on the test statistic of the L-test for normality at the significance level 0.05. The distribution with the maximum test statistic value has the least Gaussian distribution. In order to represent the spike frame feature at full scales, feature coefficients were selected from different levels. The number of the feature coefficient candidates for each level is one-fourth the coefficient number of each level, which is 1 for A4, 1 for D4, 2 for D3, 4 for D2 and 8 for D1. Coefficients with the first n (depending on the level) maximum test statistic values were selected as the candidates. Table IV shows the feature coefficient candidates for each data set in test statistic value descending order. The feature coefficients were selected from the candidates according to criteria that the null hypothesis should be rejected and the test statistic value should be in the first 20 maximum values of all the coefficients. The selected feature coefficients are in bold in Table IV.

Based on the selected feature coefficients, feature vectors can be generated for each spike frame. Also take Easy 1 (noise level 0.05) data set for example. Fig. 8(a) shows the mapping of the

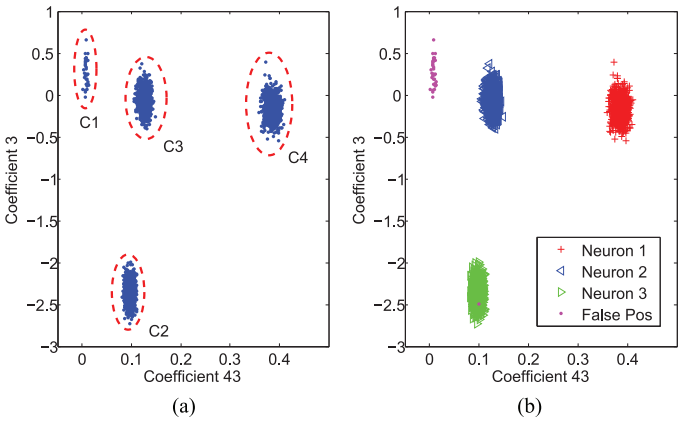

Fig. 8. (a) Mapping of the feature vectors on the feature coefficients space as seen by the cluster. (b) Mappings are color-coded to distinguish between neurons and false positives.

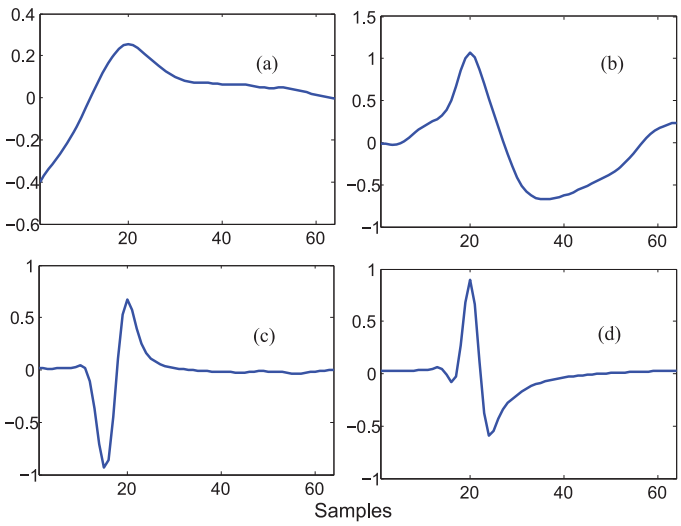

Fig. 9. (a) Average frame waveform of class C1 in Fig. 7. (b) Average frame waveform of class C2 in Fig. 7. (c) Average frame waveform of class C3 in Fig. 7. (d) Average frame waveform of class C4 in Fig. 7.

feature vectors on the feature coefficients space with coefficient 43 on the x-axis and coefficient 3 on the y-axis, as seen by the cluster. Fig. 8(b) shows the color-coded mapping to distinguish between the three neurons and the false positives, using prior knowledge from the data sets. In Fig. 8(a), it is obvious that the spikes can be divided into four classes, indicated by C1, C2, C3, and C4. Average frame waveforms for each class have been presented in Fig. 9. We can deduce from Fig. 9 that the class C1 is a false positive class based on the prior knowledge of the action potential waveform, whereas class C2, C3, and C4 are action potentials from different neurons. Therefore, spikes in class C1 can be eliminated, and the S_p of the spike detecting algorithm can be improved further. Note that the dimension of the feature vector in data set Easy 1 (0.05) is 16. Only two dimensions of the feature vector are presented in Fig. 8.

Feature vectors were divided into several classes based on the k-means method, and the results are shown in Table V. Note that the false positives have also been input into the cluster and treated as a single class.

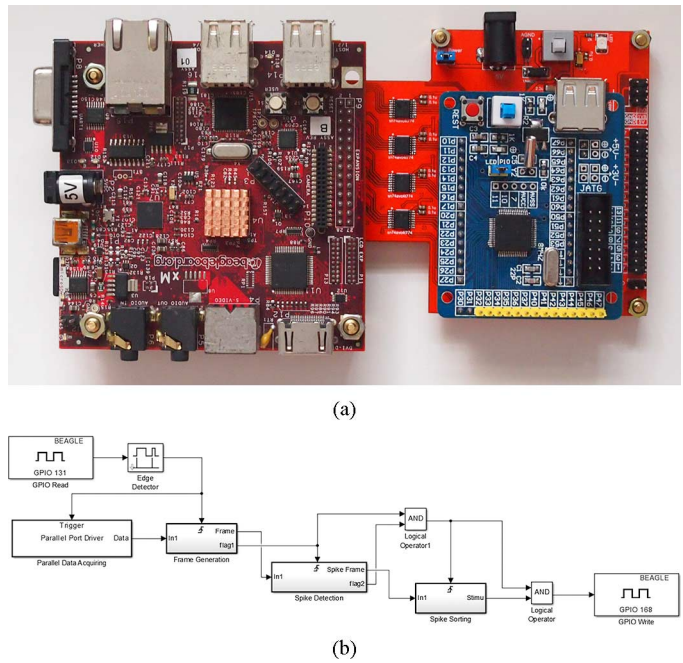

Fig. 10. (a) Photograph of the controller (right) and the digital signal processer (left) of the MENB prototype system. (b) Verified signal processing model for downloading.

In comparison with the other methods in Table V, the method presented in this study has the highest average clustering accuracy. However, it is hard to define the best method, since the clustering accuracy of the method depends on the test data. For example, Method II performs better than Method IV in data set Easy 2 (0.10) and Hard 2 (0.10). In general, the method with DWT performs better than the method with principle component analysis (PCA) based on the comparison between Methods I and III. The reason could be that the PCA selects the eigenvectors accounting for the largest variance of the data, but these directions do not necessarily provide the best separation of the spike classes. By contrast, selecting features based on their probity distribution provides better performance. The comparison between Methods III and IV indicates that k-means clustering method with Mahalanobis distance performs better than k-means with Euclidean distance, which has also been found by literature [56], [57].

Based on the parameters obtained from the training phase, the prototype system in the bridging phase has been tested in real time. The photograph of the controller (including the A-D and D-A converter) and the digital signal processer of the MENB prototype system are shown in Fig. 10(a). We built the signal processing part of the prototype system with the rapid prototyping technology based on Simulink and open source hardware Beagleboard-XM. The main processor of the Beagleboard-XM is DM3730 (1 GHz ARM Cortex™-A8 core and 800 MHz TMS320C64x+™ DSP Core). After some driver development, the signal processing model verified in Simulink can be downloaded to the hardware directly. This technology reduces the gap between algorithm design and hardware implementation.

The input simulated neural signal was generated by an arbitrary waveform generator designed by us. The waveforms in the

TABLE V
CLUSTERING RESULTS

Data Set (Noise)	Number of Spikes	(I)PCA+k-means[a]		(II)Wavelet+SPC[b]		(III)Wavelet+k-means[c]		(IV)Wavelet+k-means[d]	
		Error Number	Accuracy (%)	Error Number	Accuracy (%)[e]	Error Number	Accuracy (%)	Error Number	Accuracy (%)
Easy 1(0.05)	2765(36)	0(1)	99.96	1	99.96	0(1)	99.96	0(1)	99.96
Easy 1(0.10)	2786(33)	0(5)	99.82	5	99.82	0(4)	99.86	0(4)	99.86
Easy 1(0.15)	2716(43)	263(5)	90.13	5	99.81	0(2)	99.93	0(2)	99.93
Easy 1(0.20)	2194(129)	465(122)	73.25	12	99.55	3(4)	99.68	2(7)	99.59
Easy 2(0.05)	2634(15)	0(0)	100	3	99.89	0(0)	100	0(0)	100
Easy 2(0.10)	2700(8)	488(5)	81.74	10	99.63	523(7)	80.37	694(7)	74.04
Easy 2(0.15)	2621(26)	704(12)	72.68	45	98.30	182(3)	92.94	135(3)	94.73
Easy 2(0.20)	1734(21)	645(21)	61.59	306	88.73	189(2)	88.99	16(1)	99.02
Hard 1(0.05)	2632(16)	0(0)	100	0	100	0(0)	100	0(0)	100
Hard 1(0.10)	2652(15)	595(6)	77.34	41	98.45	60(2)	97.66	0(2)	99.92
Hard 1(0.15)	2661(30)	1456(1)	45.25	81	96.95	334(2)	87.37	0(2)	99.92
Hard 1(0.20)	2034(68)	1557(1)	23.40	651	75.19	414(2)	79.55	0(2)	99.90
Hard 2(0.05)	2551(16)	4(0)	99.84	1	99.96	9(0)	99.65	0(0)	100
Hard 2(0.10)	2748(6)	882(5)	67.72	8	99.71	670(5)	75.44	549(4)	79.88
Hard 2(0.15)	2605(2)	1114(1)	57.20	443	83.16	1431(2)	44.99	473(0)	81.84
Hard 2(0.20)	1926(8)	1016(6)	46.94	1462	46.17	638(3)	66.72	26(2)	98.55
Average			74.80		92.83		88.32		95.45

Notes: Numbers in brackets are for false positives. Overlapping spikes are not considered. Roman Number in brackets indicates the method number
[a]This method has been used in literature [53]. First four principle components were used as the feature vector and k-means method based on Euclidean distance.
[b]Quiroga used this method in his study, results are obtained from his study[44]. Superparamagetic clustering (SPC) is a clustering method.
[c]Method presented in this study. The k-means clustering method is based on Euclidean distance.
[d]Method presented in this study. The k-means clustering method is based on Mahalanobis distance.
[e]The sorting accuracy calculation for this method is based on the number of spikes and error number in reference [44].

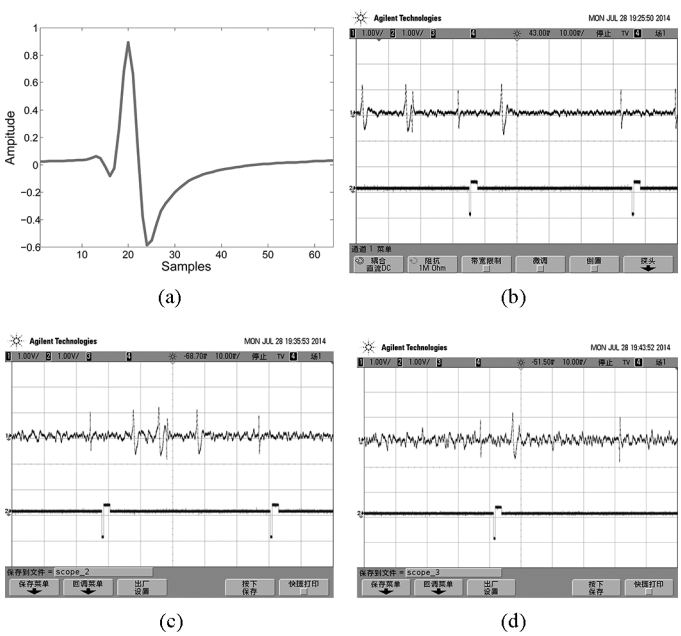

Fig. 11. (a) Spike waveform of the spike to be bridged. (b) Part of the test waveforms for data set Easy 1 (noise level 0.05). (c) Part of the test waveforms for data set Easy 1 (noise level 0.10). (d) Part of the test waveforms for data set Easy 1 (noise level 0.15).

TABLE VI
3-FOLD CROSS-VALIDATION RESULT

Data Set	S_n(%)	S_p(%)	Accuracy(%)[a]	Accuracy(%)[b]
Easy 1(0.05)	100	99.18	99.82	94.63
Easy 1(0.10)	100	98.80	99.53	99.64
Easy 1(0.15)	100	95.52	98.45	99.72
Easy 1(0.20)	99.59	93.90	94.82	90.78
Easy 2(0.05)	99.96	100	99.62	99.62
Easy 2(0.10)	99.96	99.42	96.74	92.99
Easy 2(0.15)	99.96	96.21	97.65	99.24
Easy 2(0.20)	96.17	96.01	93.69	96.28
Hard 1(0.05)	100	99.36	99.78	99.18
Hard 1(0.10)	100	99.32	97.56	99.62
Hard 1(0.15)	99.96	97.69	87.88	98.75
Hard 1(0.20)	99.21	95.26	80.99	94.14
Hard 2(0.05)	99.96	99.49	99.29	99.57
Hard 2(0.10)	99.96	98.58	70.61	83.51
Hard 2(0.15)	100	97.26	82.35	97.73
Hard 2(0.20)	96.10	97.13	73.31	98.03
Average	99.43	97.70	92.00	96.46

Notes: Overlapping spikes are not considered for the S_n, S_p, and classification accuracy calculation
[a] Using the Euclidean distance as the metrics
[b] Using the Mahalanobis distance as the metrics

tests have been recorded by the oscilloscope DSO7034A (Agilent Inc., CA, USA), and parts of the waveforms have been presented in Fig. 11(b)–(d). Fig. 11(a) is the spike waveform to be bridged. From Fig. 11(b)–(d), the upper waveform is the input signal (data set Easy 1 noise level 0.05, 0.10, 0.15) for the spike detecting and sorting algorithm. The lower waveform is the D-A converter output. From Fig. 11(b)–(d), we can observe that only spikes with a waveform in Fig. 11(a) will trigger a charge balanced waveform for stimulation. The delay between the spike and the stimulating waveform is about 5 ms due to the signal processing time.

Finally, the three-fold cross-validation method has been used to evaluate the prototype system performance. Each data set was partitioned into three complementary subsets. In one round, two subsets were used for the training phase, and one subset was used for the bridging phase. Multiple rounds were performed using different subsets for training and bridging phase. The average sensitivity, specificity, and accuracy in the bridging phase for each data set were calculated as shown in Table VI. Both Euclidean distance and Mahalanobis distance have been used

for calculating the distance between the input spike frame feature vector and class feature vector in the bridging phase. For the calculation of the Mahalanobis distance, we used the covariance matrix in the training phase as the estimation of the covariance matrix in the bridging phase. The average S_{n} and S_{p} are 99.43% and 97.70%, respectively, which is almost the same as in Table III. The average classification accuracy is 92.00% using Euclidean distance and 96.46% using Mahalanobis distance. The result shows that covariance matrix in the training phase is a good estimation for the covariance matrix in the training phase. However, using the Mahalanobis distance increases additional 4096 multiplications each time for distance calculation, which may be a great burden to the processor, especially for the multichannel signal processing.

IV. Conclusion

In this paper, the concept of the MENB aiming to regenerate neural signal and rebuild motor function of the paralyzed limbs has been presented. This study focused on the prototype system design of the MENB. In comparison with the previous MENB systems [40], [58], this prototype system regenerates neural signals with spike identification. Only the spikes of the neuron to be bridged will initiate the stimuli. The performance of the system has also been evaluated based on the extracellular recording neural signal data base available at Caltech both in training phase and bridging phase. The average sensitivity and specificity are 99.43% and 97.83%. The average clustering accuracies in training phase and classification accuracy in bridging phase are 95.45% and 96.46%, respectively.

However, there are also many challenges for the MENB, such as how to implant the electrode array into the spinal cord, how to fix the electrode array, how to select the right neuron to be bridged, how to choose the location for stimulation, and how to deal with the influence of the instability of unit activity, amplitude and waveform shape over time. Some of these problems are under study such as the functional localization of spinal cord [59]. Many further works need to be done to make the concept of MENB feasible for clinical practice.

Besides, the prototype system also needs to be improved. For a real MENB system, it should be an implanted system. Therefore the power consumption should be considered as an important constraint. The European standards require that the surface of the implant not to exceed 1°C above body temperature [60]. In this study, we did not consider the power consumption constraint. The quiescent dissipation of the neural signal detecting circuit seems to be high (56.28 mW), although it has a good performance in noise and CMRR. In order to reduce the power consumption of the neural signal detecting circuit, the behavioral model of the circuit should be built for analyzing the minimum requirements for accurate and efficient spike detecting and sorting [61], [62]. Application-specific integrated circuit for the MENB should be designed based on the minimum requirements. The control algorithm and spike detecting and sorting algorithm should also be optimized, especially for multichannel applications. In addition, the 2.4 GHz low cost transceiver CC2500 used in the prototype system for wireless data recording is only applicable for one channel transmission restricted by the maximum data rate of 500 kb/s. New transceivers based on Bluetooth 4.0 with a maximum data rate 24 Mbps will replace the CC2500 in the future.

Acknowledgment

The authors would like to thank Dr. K.-C. Wang, IEEE Fellow, Prof. Z.-L. Jiang from Nantong University and anonymous reviewers for helpful comments and suggestions. The authors would also like to thank Prof. R. Q. Quiroga from University of Leicester for useful data and kind help.

References

[1] [Online]. Available: http://www.christopherreeve.org/site/c.ddJFKRNoFiG/b.5102631/k.6C44/Prevalence_of_Paralysis.htm

[2] B. S. Bregman, E. Kunkel-Bagden, L. Schnell, H. N. Dai, D. Gao, and M. E. Schwab, "Recovery from spinal cord injury mediated by antibodies to neurite growth inhibitors," *Nature*, vol. 378, pp. 498–501, 1995.

[3] M. Thallmair, G. A. S. Metz, W. J. Z'Graggen, O. Raineteau, G. L. Kartje, and M. E. Schwab, "Neurite growth inhibitors restrict plasticity and functional recovery following corticospinal tract lesions," *Nature Neurosci.*, vol. 1, pp. 124–131, 1998.

[4] P. Moissonnier, T. Reviron, J. H. Ye, and J. C. Horva, "Motoneurons of the injured spinal cord of the adult dog can grow lengthy axons into an autologous peripheral nerve graft: A retrograde axonal tracing study," *Spinal Cord*, vol. 34, no. 6, pp. 320–325, 1996.

[5] Y. S. Lee, C. Y. Lin, R. T. Robertson, I. Hsiao, and V. W. Lin, "Motor recovery and anatomical evidence of axonal regrowth in spinal cord-repaired adult rats," *J. Neuropathol. Exp. Neurol.*, vol. 63, pp. 233–245, 2004.

[6] P. S. Diener and B. S. Bregman, "Fetal spinal cord transplants support the development of target reaching and coordinated postural adjustments after neonatal cervical spinal cord injury," *J. Neurosci.*, vol. 18, no. 2, pp. 763–778, 1998.

[7] A. Pinzon, B. Calancie, M. Oudega, and B. Noga, "Conduction of implulses by axons regenerated in a Schwann cell graft in the transected adult rat spinal cord," *J. Neurosci. Res.*, vol. 64, pp. 533–541, 2001.

[8] T. Takami, M. Oudegal, M. L. Bates, P. M. Wood, N. Kleitman, and M. B. Bungle, "Schwann cell but not olfactory ensheathing glia transplants improve hindlimb locomotor performance in the moderately contused adult rat thoracic spinal cord," *J. Neurosci.*, vol. 22, pp. 6670–6681, 2002.

[9] Y. Li, P. M. Field, and G. Raisman, "Repair of adult rat corticospinal tract by transplants of olfactory ensheathing cells," *Science*, vol. 277, no. 5334, pp. 2000–2002, 1997.

[10] Y. Li, P. Decherchi, and G. Raisman, "Transplantation of olfactory ensheathing cells into spinal cord lesions restores breathing and climbing," *J. Neurosci.*, vol. 23, pp. 727–731, 2003.

[11] H. S. Keirstead, G. Nistor, G. Bernal, M. Totoiu, F. Cloutier, K. Sharp, and O. Steward, "Human embryonic stem cell-derived oligodendrocyte progenitor cell transplants remyelinate and restore locomotion after spinal cord injury," *J. Neurosci.*, vol. 25, no. 19, pp. 4694–4705, 2005.

[12] S. S. Schultz, "Adult stem cell application in spinal cord injury," *Curr. Drug Targets*, vol. 6, pp. 63–73, 2005.

[13] E. R. H. M. Tuszynski, "Neurotrophins: Potential therapeutic tools for the treatment of spinal cord injury," *J. Amer. Soc. Experimental Neurotherapeutics*, vol. 8, no. 4, pp. 694–703, 2011.

[14] Y. Zhang, F. Y. Gao, D. S. Wu, P. Moshayedi, X. Y. Zhang, H. Ellamushi, J. Yeh, J. V. Priestley, and X. N. Bo, "Lentiviral mediated expression of a NGF-soluble Nogo receptor 1 fusion protein promotes axonal regeneration," *Neurobiol. Dis.*, vol. 58, pp. 270–280, 2013.

[15] S. Franz, "Gene therapy approaches to enhancing plasticity and regeneration after spinal cord injury," *Exp. Neurol.*, vol. 235, no. 1, pp. 62–69, 2012.

[16] K. Zukor, "Short hairpin RNA against PTEN enhances regenerative growth of corticospinal tract axons after spinal cord injury," *J. Neurosci.*, vol. 33, no. 39, pp. 15350–15361, 2013.

[17] D. X. Ban, "Combination of activated Schwann cells with bone mesenchymal stem cells: The best cell strategy for repair after spinal cord injury in rats," *Regenerative Medicine*, vol. 6, no. 6, pp. 707–720, 2011.

[18] D. D. Pearse, F. C. Pereira, A. E. Marcillo, M. L. Bates, Y. A. Berrocal, M. T. Filbin, and M. B. Bunge, "cAMP and Schwann cells promote axonal growth and functional recovery after spinal cord injury," *Nature Med.*, vol. 10, pp. 610–616, 2004.

[19] J. G. Boyd, R. Doucette, and M. D. Kawaja, "Defining the role of olfactory ensheathing cells in facilitating axon remyelination following damage to the spinal cord," *FASEB J.*, vol. 19, pp. 694–703, 2005.

[20] W. Murrell, F. Féron, A. Wetzig, N. Cameron, K. Splatt, B. Bellette, J. Bianco, C. Perry, G. Lee, and A. Mackay-Sim, "Multipotent stem cells from adult olfactory mucosa," *Dev. Dyn.*, vol. 233, pp. 496–515, 2005.

[21] S. Koshizuka, S. Okada, A. Okawa, M. Koda, M. Murasawa, M. Hashimoto, T. Kamada, K. Yoshinaga, M. Murakami, H. Moriya, and M. Yamazaki, "Transplanted hematopoietic stem cells from bone marrow differentiate into neural lineage cells and promote functional recovery after spinal cord injury in mice," *J. Neuropathol. Exp. Neurol.*, vol. 63, pp. 64–72, 2004.

[22] M. J. Amador and J. D. Guest, "An appraisal of ongoing experimental procedures in human spinal cord injury," *J. Neurol. Phys. Ther.*, vol. 29, pp. 70–86, 2005.

[23] D. D. Pearse, A. E. Marcillo, M. Oudega, M. P. Lynch, P. M. Wood, and M. B. Bunge, "Transplantation of Schwann cells and olfactory ensheathing glia after spinal cord injury: Does pretreatment with methylprednisolone and interleukin-10 enhance recovery?," *J. Neurotrauma*, vol. 21, pp. 1223–1239, 2004.

[24] S. Thuret, L. D. F. Moon, and F. H. Gage, "Therapeutic interventions after spinal cord injury," *Nature*, vol. 7, pp. 628–643, 2006.

[25] V. Dietz and S. J. Harkema, "Locomotor activity in spinal cord-injured persons," *J. Appl. Physiol.*, vol. 96, no. 5, pp. 1954–1960, 2004.

[26] S. Yen, B. D. Schmit, J. M. Landry, H. Roth, and M. Wu, "Locomotor adaptation to resistance during treadmill training transfers to overground walking in human SCI," *Exp. Brain Res.*, vol. 216, no. 3, pp. 473–482, 2012.

[27] P. Sale, M. Franceschini, A. Waldner, and S. Hesse, "Use of the robot assisted gait therapy in rehabilitation of patients with stroke and spinal cord injury," *Eur. J. Phys. Rehabil. Med.*, vol. 48, no. 1, pp. 111–121, 2012.

[28] R. D. de Leon, M. D. Kubasak, P. E. Phelps, W. K. Timoszyk, D. J. Reinkensmeyer, R. R. Roy, and V. R. Edgerton, "Using robotics to teach the spinal cord to walk," *Brain Res. Rev.*, vol. 40, no. 1, pp. 267–273, 2002.

[29] J. A. Nessler, K. Minakata, K. Sharp, and D. J. Reinkensmeyer, "Robot-assisted hindlimb extension increases the probability of swing initiation during treadmill walking by spinal cord contused rats," *J. Neurosci. Meth.*, vol. 159, no. 1, pp. 66–77, 2007.

[30] K. J. Hutchinson, F. Gómez Pinilla, M. J. Crowe, Z. Ying, and D. M. Basso, "Three exercise paradigms differentially improve sensory recovery after spinal cord contusion in rats," *Brain*, vol. 127, no. 6, pp. 1403–1414, 2004.

[31] N. L. van Meeteren, R. Eggers, A. J. Lankhorst, W. H. Gispen, and F. P. Hamers, "Locomotor recovery after spinal cord contusion injury in rats is improved by spontaneous exercise," *J. Neurotraum*, vol. 20, no. 10, pp. 1029–1037, 2003.

[32] M. S. Nash, "Exercise as a health-promoting activity following spinal cord injury," *J. Neurol. Phys. Ther.*, vol. 29, no. 2, pp. 87–103,106, 2005.

[33] G. Zeilig, H. Weingarden, M. Zwecker, I. Dudkiewicz, A. Bloch, and A. Esquenazi, "Safety and tolerance of the ReWalk™ exoskeleton suit for ambulation by people with complete spinal cord injury: A pilot study," *J. Spinal Cord Med.*, vol. 35, no. 2, pp. 101–196, 2012.

[34] K. T. Ragnarsson, "Functional electrical stimulation after spinal cord injury: Current use, therapeutic effects and future directions," *Spinal Cord*, vol. 46, no. 4, pp. 255–274, 2007.

[35] J. K. Chapin, K. A. Moxon, R. S. Markowitz, and M. A. Nicolelis, "Real-time control of a robot ARM using simultaneously recorded neurons in the motor cortex," *Nat. Neurosci.*, vol. 2, no. 7, pp. 664–670, 1999.

[36] L. R. Hochberg, M. D. Serruya, G. M. Friehs, J. A. Mukand, M. Saleh, A. H. Caplan, A. Branner, D. Chen, R. D. Penn, and J. P. Donoghue, "Neuronal ensemble control of prosthetic devices by a human with tetraplegia," *Nature*, vol. 442, no. 7099, pp. 164–171, 2006.

[37] Z. G. Wang, X. S. Gu, and X. Y. Lü, "Neural channel bridge aided by a micro-electronic system," US patent, US 8,000,806 B2, 2011.

[38] B. Clark and M. Häusser, "Neural coding: Hybrid analog and digital signaling in axons," *Curr. Bio.*, vol. 16, no. 5, 2006.

[39] H. Lodish *et al., Molecular Cell Biology*, 4th ed. New York, NY, USA: W. H. Freeman, 2000.

[40] Z. H. Huang, Z. G. Wang, X. Y. Lü, W. Y. Li, X. Y. Shen, X. T. Zhao, S. S. Xie, H. X. Pan, and C. L. Zhu, "Design and experiment of a neural signal detection using a FES driving system," in *Proc. IEEE Eng. Med. Bio (EMBC)*, Buenos Aires, Argentina, 2010, pp. 1523–1526.

[41] A. C. Metting van Rijn, A. Peper, and C. A. Grimbergen, "High-quality recording of bioelectric events: Part 1 interference reduction, theory and practice," *Med. Bioi. Eng. Comput.*, vol. 28, pp. 389–397, 1990.

[42] C. Kitchin, Reducing RFI Rectification Errors in In-Amp Circuits, Analog Devices, Inc., 2003, Application Note (AN-671).

[43] D. R. Merrill, M. Bikson, and J. G. Jefferys, "Electrical stimulation of excitable tissue: Design of efficacious and safe protocols," *J. Neurosci. Meth.*, vol. 141, no. 2, pp. 171–198, 2005.

[44] R. Q. Quiroga, Z. Nadasdy, and Y. Ben-Shaul, "Unsupervised spike detection and sorting with wavelets and superparamagnetic clustering," *Neural Comput.*, vol. 16, no. 8, pp. 1661–1687, 2004.

[45] J. P. Welsh, C. Schwarz, and M. Nicolelis, "Multielectrode recording from the cerebellum," *Meth. Neural Ensemble Rec.*, vol. 5, pp. 79–100, 1999.

[46] K. H. Kim and S. J. Kim, "Neural spike sorting under nearly 0-dB signal-to-noise ratio using nonlinear energy operator and artificial neural-network classifier," *IEEE Trans. Biomed. Eng.*, vol. 47, no. 10, pp. 1406–1411, Oct. 2000.

[47] J. H. Choi, H. K. Jung, and T. Kim, "A new action potential detector using the MTEO and its effects on spike sorting systems at low signal-to-noise ratios," *IEEE Trans. Biomed. Eng.*, vol. 53, no. 4, pp. 738–746, Apr. 2006.

[48] D. L. Donoho and J. M. Johnstone, "Ideal spatial adaptation by wavelet shrinkage," *Biometrika*, vol. 81, no. 3, pp. 425–455, 1994.

[49] R. Q. Quiroga, "Spike sorting," *Scholarpedia*, vol. 2, no. 12, p. 3583, 2007.

[50] H. W. Lilliefors, "On the Kolmogorov-Smirnov test for normality with mean and variance unknown," *J. Amer. Stat. Assoc.*, vol. 62, no. 318, pp. 399–402, 1967.

[51] H. Jiawei and M. Kamber, *Data Mining: Concepts and Techniques*. San Francisco, CA, USA: Morgan Kaufmann, 2001, vol. 5.

[52] J. C. Letelier and P. P. Weber, "Spike sorting based on discrete wavelet transform coefficients," *J. Neurosci. Meth.*, vol. 101, no. 2, pp. 93–106, 2000.

[53] M. S. Lewicki, "A review of methods for spike sorting: The detection and classification of neural action potentials," *Network: Comput. Neural Syst.*, vol. 9, no. 4, pp. R53–R78, 1998.

[54] X. T. Zhao, Z. G. Wang, and X. Y. Lü, "Effects of microelectrode array configuration and position on the threshold in electrical extracellular stimulation of single nerve fiber: A modeling study," *Prog. Electromagn. Res. B*, vol. 55, pp. 401–419, 2013.

[55] [Online]. Available: http://www.vis.caltech.edu/~rodri/data.htm

[56] A. M. Kamboh and A. J. Mason, "Computationally efficient neural feature extraction for spike sorting in implantable high-density recording systems," *IEEE Trans. Neural Syst. Rehabil. Eng.*, vol. 21, no. 1, pp. 1–9, Jan. 2013.

[57] K. D. Harris, D. A. Henze, J. Csicsvari, H. Hirase, and G. Buzsáki, "Accuracy of tetrode spike separation as determined by simultaneous intracellular and extracellular measurements," *J. Neurophysiol.*, vol. 84, no. 1, pp. 401–414, 2000.

[58] Z. G. Wang, X. Y. Lü, W. Y. Li, X. Y. Shen, Z. H. Huang, X. T. Zhao, L. J. Du, Z. L. Jiang, X. Y. Gao, G. H. Wang, H. X. Pan, C. L. Zhu, X. Gong, and L. Qiu, "Signal regeneration and function rebuilding using microelectronic neural bridge between two far-separated nervous systems," in *Proc. Int. Conf. Body Sensor Networks*, Dallas, TX, USA, 2011, pp. 25–28.

[59] W. Huang, X. Y. Shen, and T. P. Huang, "Experimental research on the reference coordinates for functional localization of spinal cord," in *Int. Conf. Bioinform. Biomed. Eng.ineering (iCBBE)*, Shanghai, China, 2012, pp. 245–248.

[60] J. D. Weiland, W. Liu, and M. S. Humayun, "Retinal prosthesis," *Annu. Rev. Biomed. Eng.*, vol. 7, pp. 361–401, 2005.

[61] D. Y. Barsakcioglu, L. Yan, P. Bhunjun, J. Navajas, A. Eftekhar, A. Jackson, R. Quian Quiroga, and T. G. Constandinou, "An analogue front-end model for developing neural spike sorting systems," *IEEE Trans. Biomed. Circuits Syst.*, vol. 8, no. 2, pp. 216–227, Aug. 2014.

[62] J. Navajas, D. Y. Barsakcioglu, A. Eftekhar, A. Jackson, T. G. Constandinou, and Q. R. Quian, "Minimum requirements for accurate and efficient real-time on-chip spike sorting," *J. Neurosci. Meth.*, vol. 230, pp. 51–64, 2014.

Zong-Hao Huang received the B.S. degree (with honors) in electric engineering from Southeast University, Nanjing, China, in 2007, and the Ph.D. degree at the Institute of RF & OE-ICs, Southeast University, in 2015.

His research interests include electrical system design, rehabilitation engineering and digital signal processing. Since 2015, he has worked in Huawei Technologies Co., Ltd for key technologies in the fifth generation of mobile communication.

Zhi-Gong Wang (SM'93) was born in Henan, China. He received the M.-Eng. degree in radio engineering from Nanjing Institute of Technology (now, Southeast University), Nanjing, China, in 1981, and the Dr.-Ing. degree in electronic engineering from Ruhr-University Bochum, Germany, in 1990.

From 1977 to 1981, he worked on radio communication techniques and computer aided circuit designs at Nanjing Institute of Technology. From 1985 to 1990, he worked on high-speed silicon bipolar circuit designs for multigigabit/s optic fiber communication in Ruhr-University Bochum, Germany. From 1990 to 1997, he was with Fraunhofer-Institute of Applied Solid State Physics, Freiburg, Germany, working on high-speed GaAs ICs for optic-fiber data transmission and MMICs. Since Oct. 1997, he has been a Full Professor at Southeast University, Nanjing, China.

Xiao-Ying Lü was born in Shanghai, China. She received her M.-Med. degree from Shanghai Second Medical University, in 1986, and her Dr.-Dent. degree from Freiburg University, Freiburg, Germany, in 1996.

From 1996 to 1997. she was a Postdoctoral Researcher at Freiburg University, Freiburg, Germany. In 1997, she became an Associate Professor of Southeast University, China, and since 2003 she has been a Full Professor.

Wen-Yuan Li was born in Shandong, China, in 1964. He received the Master degree in 1991 from the Southeast University and the Doctor degree in 2007.

He joined Southeast University in 1991. His research areas include signals, circuits, and system; high speed IC design; analog IC design; as well as biochips.

Yu-Xuan Zhou received the B.S. degree in mechanical engineering and automation from Nanjing University of Science and Technology, Nanjing, China, in 2007, and the M.S. degree in biomedical engineering from Nanjing Medical University, Nanjing, China, in 2010. He is currently working toward the Ph.D. degree in biomedical engineering at Southeast University, Nanjing, China.

His research interests include the biomedical signal processing, neuroprosthesis system design and rehabilitation engineering.

Xiao-Yan Shen was born in 1969. She received her M.-Eng. degree from Nanjing University of Science and Technology in 2002, and the Dr.-Ing. degree in 2011 from Southeast University.

She is currently a Professor at Nantong University, Nantong, China. Her research interests are micro-electronic systems for biomedical applications.

Xin-Tai Zhao was born in Hebei Province, China, in 1976. He received the B.Eng. and M.Eng. degrees in communication engineering and detecting measurement technique and instrument engineering from Yanshan University, Qinhuandao, China, in 1999 and 2002, respectively, and the Ph.D. degree in electrical engineering from Xi'an Jiaotong University, Xi'an, China, in 2007. He was a Postdoctoral Researcher with the Institute of RF and Optoelectronic Integrated Circuits, Southeast University, Nanjing, China from 2007 to 2009.

He is currently a Lecturer with the Institute of RF and Optoelectronic Integrated Circuits, Southeast University, Nanjing, China. His research interests are in the areas of modeling electromagnetic fields and waves, computer-aided design of microwave devices, and the microelectrode systems dedicated to Neuroscience and health-care applications.